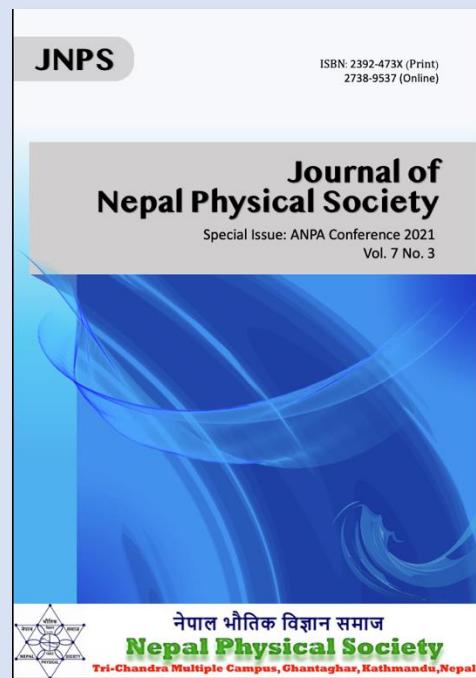# Studies of the Properties of Dust Structure Nearby the Supernova Remnants G053.41+00.3, G053.9+00.2 and G053.1+00.3 using Data from IRIS and AKARI

M. S. Paudel and S. Bhattarai

Studies of the Properties of Dust Structure Nearby the Supernova Remnants G053.41+00.3, G053.9+00.2 and G053.1+00.3 using Data from IRIS and AKARI

M. S. Paudel,[1, a)] and S. Bhattarai[2, b)]

[1)]*Department of Physics, Tri-Chandra Multiple Campus, Tribhuvan University, Nepal*
[2)]*Central Department of Physics, Tribhuvan University, Nepal*

[a)]*madhu.paudel@trc.tu.edu.np, mspaudel27@gmail.com*
[b)]*Electronic mail: surakshya.745511@cdp.tu.edu.np*

Abstract. The search of isolated dust structure is performed around the Supernova Remnants using SkyView Virtual Observatory in IRIS and AKARI survey. An isolated dust structure at Galactic Longitude: $53.54°$ and Galactic Latitude: $+0.04°$ (RA: $292.56°$, DEC: $18.24°$) nearby the Supernova Remnants G053.41+00.3, G053.9+00.2 and G053.1+00.3 is selected for this work. The intensity of infrared fluxes are extracted from the FITS image using Aladin v2.5 and v11.0 software. The dust color temperature and dust mass are calculated from infrared flux. The distribution of infrared fluxes, dust color temperature and dust mass are studied via color map and Gaussian plot using Python 3.8. The dust color temperature is found larger in IRIS data but the dust mass is found more in AKARI data. We use Gaia EDR3 for the calculation of distance to the dust structure, which is 1667.89 pc. The background sources within the dust structure is studied using SIMBAD database. The color map shows an identical distribution for infrared fluxes in both IRIS and AKARI data; but for dust color temperature and dust mass, the distribution is different. The large fluctuation of temperature indicates that dust structure is beyond the local thermodynamic equilibrium. The distribution of infrared fluxes and dust color temperature deviates from Gaussian nature, indicating the dust structure is highly affected by the background radiation sources such as, Supernova Remnants, Pulsars, etc. Study of inclination angle suggests the dust structure is non-uniform and irregular in its internal morphology. A good correlation between infrared fluxes is observed in both IRIS and AKARI data. Also, an inverse relation between dust color temperature and spectral index is observed for both data. It can be concluded that the high radiation sources within and outside the dust structure are playing major role for the asymmetrical distribution of infrared flux and dust color temperature.

INTRODUCTION

Interstellar dust is the crucial component of the interstellar medium (ISM) even though it contributes only 1% mass in ISM. It controls heating, cooling and chemical processes in ISM. It can cause the interstellar extinction by the process of absorption and scattering of radiation from nearby sources and re-radiates the absorbed radiation in infrared (IR) band contributing more than 30% luminosity in the milky way galaxy. The formation process of dust is still ongoing research in stellar astrophysics, many models have been trying to reveal the mass budget of dust in ISM. The formation of dust in late phase of

the AGB star, in the stellar wind, etc. provide the small fraction of mass budget of dust; the majority of dust are believed to be formed by the accretion and coagulation of grains in cold region of ISM. Supernova explosion is the another vital source of dust in interstellar medium that can solve the mass budgetary problem of dust in ISM. There are many works that reveal the evolution of dust during the Supernova phenomenon but it is still unclear about how and where dust grains condense and grow. The massive dust reservoir of $0.4-0.7$ $M_{\odot}$ is discovered by Matsuura *et al*. (2011) [1] by studying Supernova Remnants 1987A and another reservoir $0.1-0.2$ $M_{\odot}$ is discovered by Gomez *etal*. (2012) [2] by studying the

Crab Nebula, both using far−infrared and submillimeter observations. Gall *et al.* (2014) [3] discussed the rapid (20−240 days) formation of dust by studying the Supernova SN 2010jl in infrared observation.

Study of properties of dust around the White Dwarf [4], AGB star [5], isolated nebula [6] and cavities [7] using infrared data are very common. In this work, we have searched the isolated dust structure around the Supernova Remnants (SNR) from the catalog provided by D. A. Green (2003) [8] in Improved processing of IRAS (IRIS) [9] and AKARI [10] survey. The dust structure of size $1.5° \times 1.5°$, located at Galactic Longitude: $53.54°$ and Galactic Latitude: $+0.04°$ is selected for further investigation. This dust structure is located nearby the Supernova Remnants G053.41+00.3, G053.9+00.2 and G053.1+00.3.

DATA

In this work, we have taken data from four different sources. The IRIS [9] data at 60 μm and 100 μm are used for entire calculations. The AKARI infrared data [10] at 90 μm and 140 μm are used to compare results with IRIS data. The FITS images in both IRIS and AKARI survey are downloaded from SkyView Virtual Observatory (https://skyview.gsfc.nasa.gov) and intensity of infrared flux is extracted using Aladin v2.5 and v11.0 [11]. We used the Gaia EDR3 from Gaia Archive (https://gea.esac.esa.int/archive) for the estimation of distance to the dust structure. The SIMBAD database (http://simbad.u-strasbg.fr/simbad/sim-fcoo) are used to study the background sources within the dust structure.

METHOD

Dust Color Temperature, Dust Mass and Spectral Emissivity Index

The dust color temperature (T_d) in each pixel of a FIR image can be obtained by assuming that the dust in a single beam is isothermal and the infrared flux is due to black body radiation from dust grains at T_d, modified by a power law of spectral emissivity index. The flux density of emission from dust grain at a wavelength λ_i, is given by [12],

$$F_i = \left[\frac{2hc}{\lambda_i^3 (e^{\frac{hc}{\lambda_i K T_d}} - 1)} \right] N_d \alpha \lambda_i^{-\beta} \Omega_i \quad (1)$$

Where, N_d is the column density of dust grains, α is the constant of proportionality which relates the flux with the optical depth of the dust, β is the spectral emissivity index, and Ω_i is the solid angle subtended at λ_i by the detector.

The ratio (R) of flux density 60 μm and 100 μm can be modified by assuming that the dust emission is optically thin at 60 μm and 100 μm (i.e., $\tau_d << 1$) and that $\Omega_{60} \simeq \Omega_{100}$ [12, 13]. On further calculation, we get the expression for dust color temperature as,

$$T_d = \frac{-96}{ln\{R \times 0.6^{(3+\beta)}\}} \quad (2)$$

For AKARI data in 90 μm and 140 μm, under the similar assumptions, the expression for T_d becomes,

$$T_d = \frac{-57}{ln\{R \times 0.64^{(3+\beta)}\}} \quad (3)$$

The FITS images taken from the IRIS server in Groningen [14] and flux measurements is carried out using the Aladin v11.0. For the measurement of mass we use the longer wavelength data (100 μm for IRIS and 140 μm for AKARI) and followed the calculation of Young *et al.* (1993) [15] and Hildebrand (1983) [16]. The final expression for mass of dust is;

$$M_{dust} = 0.4 \left[\frac{S_v D^2}{B(v, T_d)} \right] \quad (4)$$

Where, S_v = f × MJy/Str × 5.288×10^{-9}, 1 MJy/Str = 1 $\times 10^{-20}$ kg s^{-2}, f is the flux density, D is the distance to the dust structure and B(v, T_d) is the Planck's function.

To calculate the mass of gas, we assume that the mass of gas is 200 times of the mass of the dust on the basis of Henning (1997) [17].

The inverse relation between β and T_d is studied following Dupac *et al.* (2003) [18]. The relation is,

$$\beta = \frac{1}{\delta + \omega T_d} \quad (5)$$

Where, δ and ω are the free parameters, with values δ= 0.40±0.02 and ω= 0.0079±0.0005K^{-1}. The value of β depends on dust grain properties like composition, size, and compactness. For example, a pure blackbody would have $\beta = 0$, the amorphous layer lattice matter has $\beta \sim 1$, and the metals and crystalline dielectrics has $\beta \sim 2$. [18]

Inclination Angle

The inclination angle (i) is the angle between the line of sight and the normal vector of the plane of the structure. This can be estimated by using Holmberg (1946) formula [19].
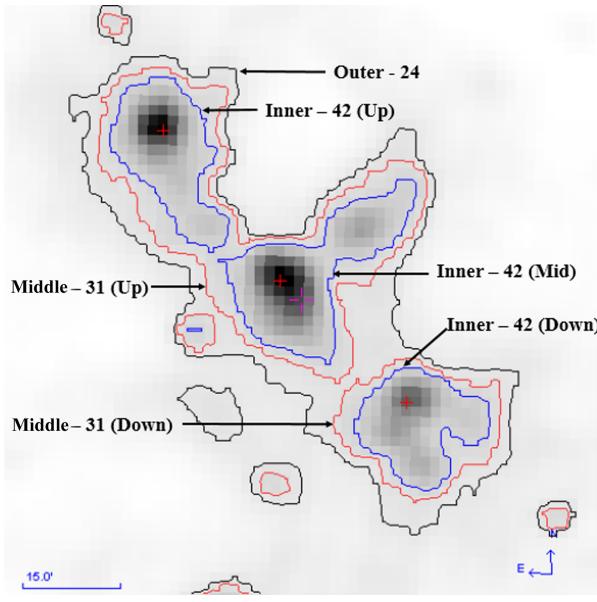
$$cos^2 i = \frac{(\frac{b}{a})^2 - q*^2}{1 - q*^2} \quad (6)$$

Where, $\frac{b}{a}$ is the ratio of minor to major axis and $q*$ is the intrinsic flatness of the structure. We used the intrinsic flatness 0.20 for the oblate spheroidal structure [20].

RESULTS & DISCUSSION

Structure

In this work, the FITS image of the dust structure having size $1.5° \times 1.5°$, located at Galactic Longitude: 53.54° and Galactic Latitude: +0.04° (RA: 292.56°, DEC:18.24°), taken from IRIS (60 μm and 100 μm) and AKARI (90 μm and 140 μm) survey are downloaded from SkyView Virtual Observatory and processed in the Aladin v2.5 and v11.0 [11] separately. The Aladin view of IRIS image at 100 μm with the different contours is shown in **FIGURE 1**. There are 3,600 pixels in IRIS data and 250,000 pixels in AKARI data. The marginal data are discarded, and the data in the range, RA: 291.97° to 293.20° and DEC: 17.67 ° to 18.88 ° are included in this work. After selecting this region the size of dust structure becomes $1.21° \times 1.23°$ and there are 2,256 pixels in IRIS data and 157,038 pixels in AKARI data.

FIGURE 1. Figure shows the $1.5° \times 1.5°$ IRIS 100 μm FITS image of dust structure located at Galactic Longitude: 53.54° and Galactic Latitude: +0.04° (RA: 292.56° and DEC:18.24°) along with the name of contours. The red cross marks represents the pixels with maximum flux within the respective contours, which are assumed to be the center of contour enclosing it.

Dust Color Temperature and Mass

The intensity of infrared flux, at 60 μm and 100 μm in IRIS data and at 90 μm and 140 μm in AKARI data, extracted from Aladin v11.0 within the selected rectangular region are used to calculate the dust color temperature according to equation (2) and (3), where we use the value of spectral emissivity index 2 assuming the dust in ISM as crystalline dielectric [18]. For the estimation of dust mass we need distance. We use Gaia EDR3 for distance estimation. We have downloaded all Gaia sources found within the dust structure and use selection criteria in parallax (ω) to remove the background ($\omega < 0.3$) and foreground ($\omega > 1.0$) sources and negative parallax ($\omega > 0$). The average distance, which is the reciprocal of parallax, of dust structure obtained using these data is 1667.89 pc. The **TABLE I.** gives the detail information of dust color temperature and dust mass within the dust structure.

The average temperature calculated using short wavelength data (IRIS, 60 μm and 100 μm) is larger than that calculated using long wavelength data (AKARI, 90 μm and 140 μm). This is contradictory to the result obtained by Jha and Aryal (2018) [7], they found that the dust color temperature using IRIS data is smaller than that calculated by using AKARI data. Our result is in accordance with the Wien's displacement law. Narrower the range of dust color temperature higher the probability of being in the thermal equilibrium [7]. The large temperature fluctuation more than 10 K in both IRIS and AKARI data suggest that the dust within the region are not in thermal equilibrium. Furthermore, the dust structure is highly affected by the background sources observed in SIMBAD database.

Estimation of dust mass shows that the mass of dust calculated by using long wavelength data is more than by using the short wavelength data. This indicates that mass of cold dust within the region is more than the mass of warm dust.

TABLE I. Comparison of Dust color temperature and mass using IRIS and AKARI data.

Quantity	IRIS	AKARI
T_{max}	$33.56 \pm 3.95\,K$	$28.86 \pm 5.56\,K$
T_{min}	$22.67 \pm 1.50\,K$	$15.78 \pm 0.98\,K$
T_{av}	$25.66 \pm 0.04\,K$	$17.74 \pm (3.42 \times 10^{-3})\,K$
Range	$10.89 \pm 2.72\,K$	$13.09 \pm 3.27\,K$
M_{dust}	$28.45\,M_{\odot}$	$5.01 \times 10^4\,M_{\odot}$
M_{gas}	$5.69 \times 10^3\,M_{\odot}$	$1.00 \times 10^7\,M_{\odot}$

Color Map: Infrared Flux, Dust Color Temperature and Dust Mass

The intensity of infrared fluxes, dust color temperature and dust mass obtained from IRIS and AKARI images are visualized using the color map as shown in **FIGURE 2**. The distribution of infrared fluxes are more or less similar in both 60 μm and 100 μm in IRIS data and 90 μm and 100 μm in AKARI data.

But there is significant difference in dust temperature and dust mass in IRIS and AKARI data. In IRIS data there is no clear relation between dust color temperature and dust mass. In some regions, the temperature and mass both are maximum but in some regions the temperature and mass shows inverse relation. However, for AKARI data there is a clear inverse relation between temperature and mass; the mass is maximum in those region where temperature is minimum and vice versa.

Linear Relation between Infrared Fluxes

The intensity of infrared fluxes at 60 μm and 100 μm in IRIS data and at 90 μm and 140 μm in AKARI data are fitted using linear regression for straight line as shown in **FIGURE 3**.

A good correlation is found between the data with regression coefficient, r = 0.87, for IRIS data and, r = 0.86, for AKARI data. The slope of the straight line represents the average ratio of fluxes at two wavelengths, which is 0.54 for IRIS and 0.78 for AKARI data. This can be used to calculate the average dust color temperature. The average temperature calculated by this method (30.28 K for IRIS and 22.93 K for AKARI) is more than the value of average temperature calculated above given in **TABLE I** for both IRIS and AKARI data.

Spectral Emissivity Index

The inverse relation between the spectral emissivity index (β) and dust color temperature (T_d) is illustrated by Dupeac *et al.* (2003) [18] by providing the hyperbolic functional relation. We have also studied the relationship between T_d and β for both data.

By varying β from 0 to 3 in the difference of 0.1, corresponding T_d is calculated. The data set (T_d, β) is plotted as shown in **FIGURE 4**. The best fit is observed for second degree parabola with r = 1.00, for both IRIS and AKARI data. For hyperbolic function r is 0.90 for IRIS and 0.89 for AKARI data, indicating a good correlation between T_d and β. The value of free parameter (δ, ω) for hyperbolic function are $(-1.77, 0.09)$ for IRIS data and $(-1.73, 0.13)$ for AKARI data. For both IRIS and

AKARI data, the inverse relation between β and T_d is observed as suggested by Dupac *et al.* (2003) [18].

Inclination Angle

To study the inclination angle (*i*), we choose the isolated dust structure and construct three contour levels in 100 μm IRIS image: Outer - 24, Middle - 31 and Inner - 42. Altogether, there are 6 contours, namely: Outer - 24, Middle - 31 (Up), Middle - 31 (Down), Inner - 42 (Up), Inner - 42 (Mid) and Inner - 42 (Down). The major and minor axis of each contour is calculated from Aladin v2.5 and the inclination angle is calculated by using the Holmberg (1946) formula [19] by taking the value of q* equal to 0.20 [20] for oblate spheroidal structure. The **TABLE II** presents the name of contours, major axis, minor axis and inclination angle. It is seen that, the inclination angle decreases from outside to inside with some fluctuation at Middle - 31 contour indicating the dust structure is irregular and non uniform in morphological point of view.

TABLE II. The table shows the name of contour, major and minor axis and corresponding inclination angle.
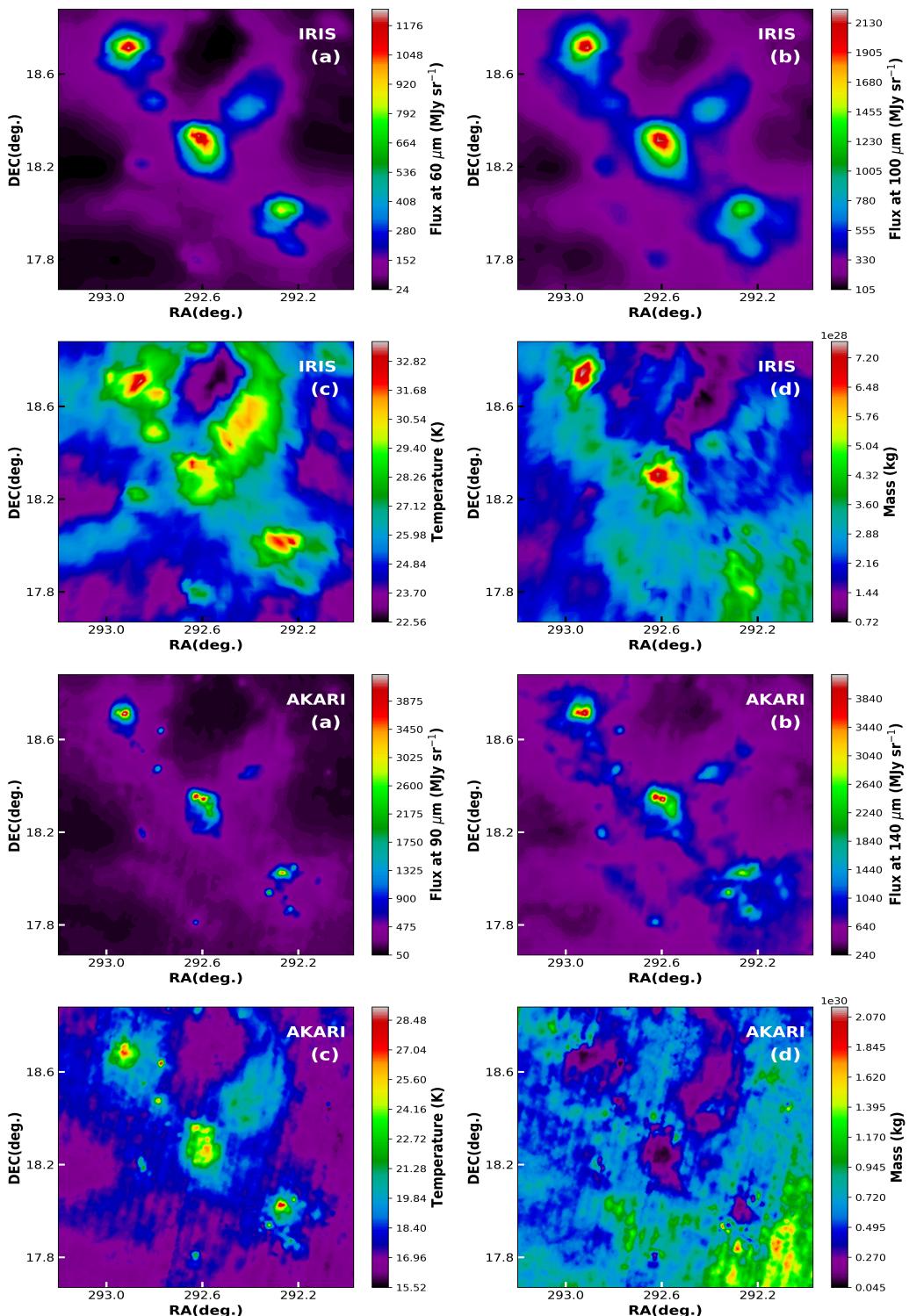
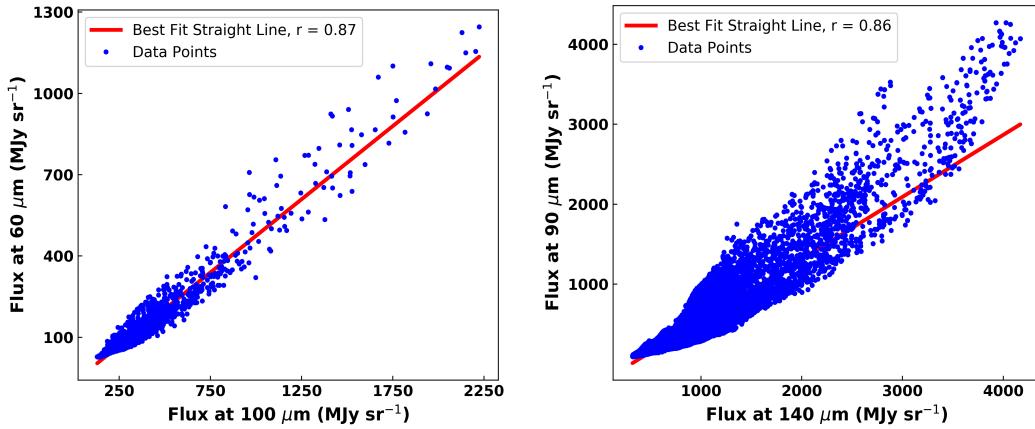| Contour	Major Axis a (arcmin)	Minor Axis b (arcmin)	Inclination Angle i (degree)
Outer$-$24	85.80	20.00	83.02
Middle$-$31 (Up)	50.06	17.26	73.38
Middle$-$31 (Down)	23.74	19.01	37.71
Inner$-$42(Up)	27.41	13.62	62.40
Inner$-$42(Mid)	33.02	14.79	62.89
Inner$-$42(Down)	18.82	11.38	54.41

Simbad Source

We studied the background sources around the dust structure using SIMBAD database. The are 1264 SIMBAD sources in rectangular region of size $1.21° \times 1.23°$, centered at RA: $292.56°$ and DEC: $18.24°$. The major sources are presented in **TABLE III**. The SIMBAD sources and data representing the coordinate of each pixels within the isolated dust structure, enclosed by Outer$-$24 contour in IRIS, are presented in **FIGURE 5**, for more clarity the sources with similar characteristics are presented in separate graph.
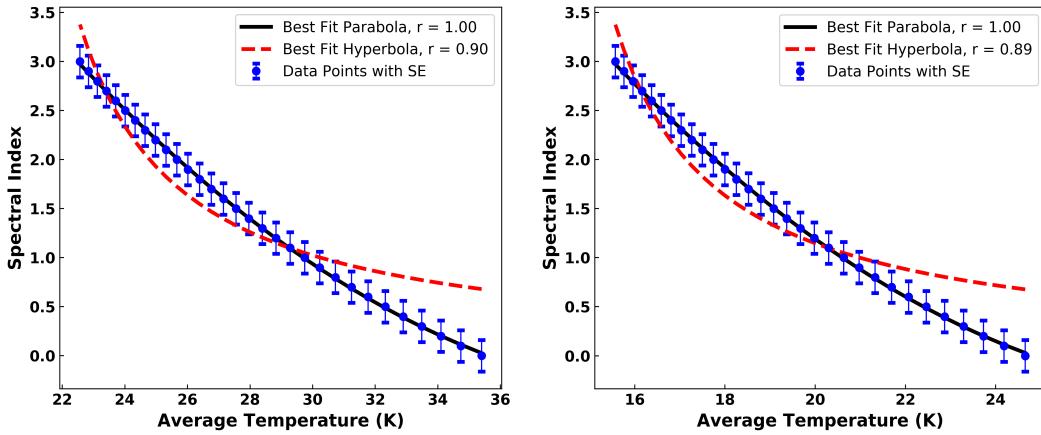
Gaussian Distribution

The distribution of intensity of infrared fluxes, dust color temperature, and dust mass based on IRIS data is studied

FIGURE 2. The color map of intensity of infrared fluxes (a and b), dust color temperature (c) and dust mass (d) in IRIS (upper 4) and AKARI data (lower 4). The distribution of fluxes is similar but the distribution of dust color temperature and dust mass are different in IRIS and AKARI data. In all plot, RA is taken along X−axis, DEC is taken along Y−axis and third variables (fluxes, temperature and mass) are taken in color bar.

FIGURE 3. Figure shows the linear relation between two infrared fluxes. The flux at 100 μm and 140 μm is taken along X$-$axis and flux at 60 μm and 90 μm is taking along Y$-$axis. Here, r represents the regression coefficient.
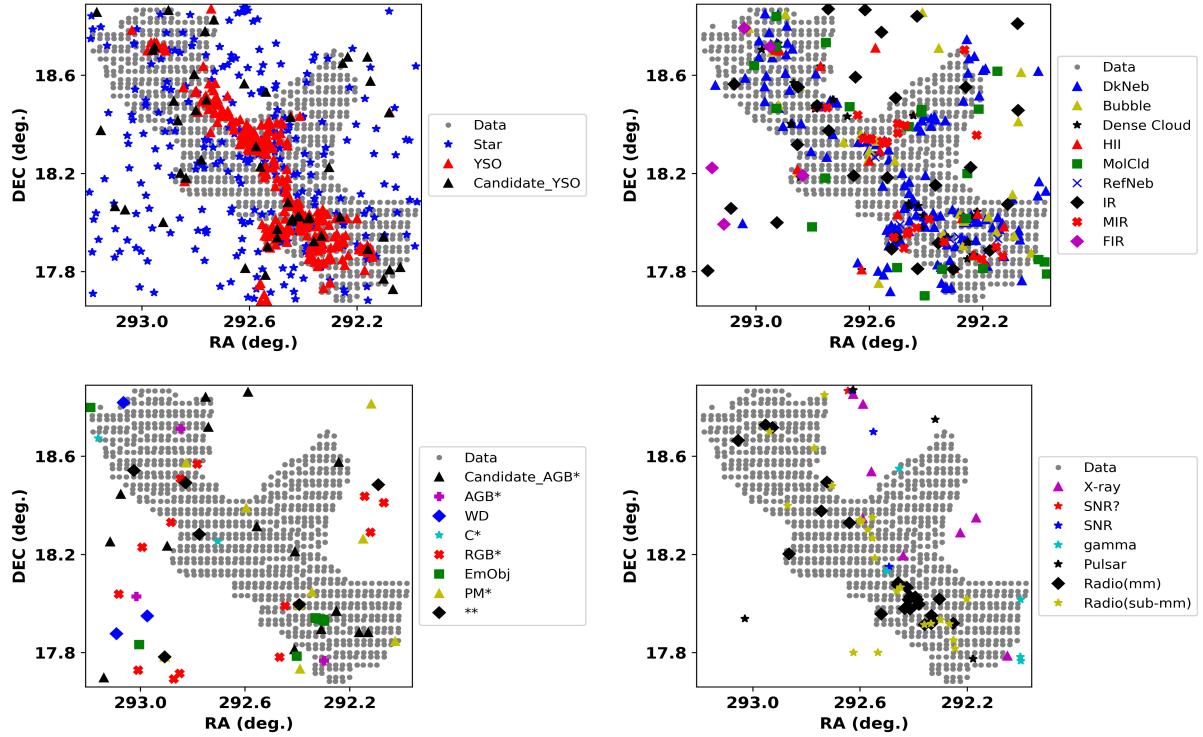

FIGURE 4. Figure shows the inverse relation between average T$_d$ along X-axis and β along Y-axis for IRIS (left) and AKARI data (right). Here, r represents the regression coefficient and SE represents the standard error.

using Gaussian modeling, which are shown in the **FIGURE 6**. The distribution of intensity of infrared fluxes are deviated heavily from Gaussian nature. The distribution of dust color temperature is deviated more in comparison to dust mass. The deviation of infrared fluxes and dust color temperature from Gaussian nature indicates high disturbance from background sources, such as, Supernova Remnant, Pulsar, X-ray and gamma ray sources, etc. Due to the effect of background sources the dust within the structure are far from the local thermodynamic equilibrium.

CONCLUSIONS

The average dust color temperature is found 25.66±0.04 K for IRIS data and 17.74±(3.42×10^{-3}) K for AKARI data. The average temperature calculated using long wavelength AKARI data is smaller than the short wavelength IRIS data. This is an usual result. The large fluctuation of temperature, more than 10 K, in both IRIS and AKARI data suggests that the dust structure is far from the local thermodynamic equilibrium, which might be due to the effect of background sources, such as, Supernova Remnants, Pulsars, X-ray and gamma ray sources, etc. The total mass of dust and gas within the dust structure is found to be more in AKARI data than the IRIS data, which is 28.45 M$_\odot$ and 5.69 × 10^3 M$_\odot$ for IRIS and 5.01× 10^4 M$_\odot$ and 1.00× 10^7 M$_\odot$ for AKARI data. The color map shows an identical distribution for infrared flux in both IRIS and AKARI data. In IRIS data, there is no any relation between dust color temperature and dust mass. However, a clear inverse relation is observed in AKARI data. Study of inclination angle suggests that the

FIGURE 5. The figure shows coordinate of pixels in IRIS within the Outer−24 contour with the major SIMBAD sources in the rectangular region of size $1.21° \times 1.23°$. The major sources are separated in four group on the basis of similar properties. In all plot, RA is taken along X−axis, DEC is taken along Y−axis

TABLE III. Major background sources taken from SIMBAD are presented below. OTYPE represents the types of source, name are given according the symbol used in SIMBAD and count represents their number. There are all together 1264 sources within the selected rectangular region.
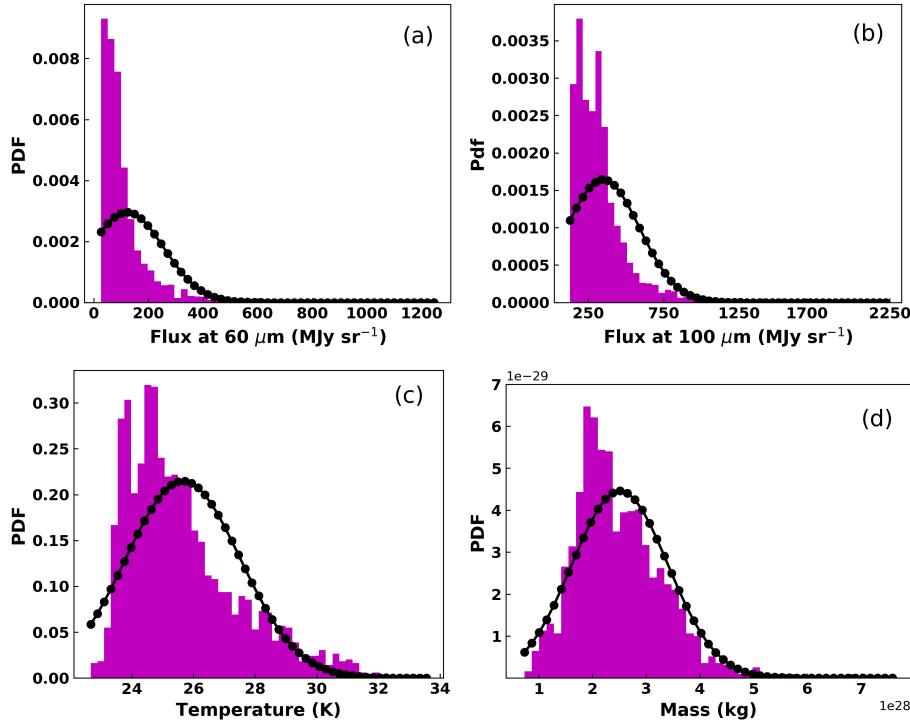
OTYPE	Count	OTYPE	Count
YSO	302	RGB*	13
Star	269	PM*	11
DkNebula	136	EmObj	9
Radio	92	X	8
Candidate-YSO	50	RfNeb	7
NIR	50	**	6
DenseCore	47	FIR	5
Bubble	30	gamma	5
IR	28	Galaxy	5
HII	27	Pulsar	4
Radio (mm)	25	Candidate-WD*	3
MIR	24	AGB*	3
Radio (sub-mm)	23	SNR	3
MolCld	22	WR*	3
Candidate-AGB*	15	SNR?	1

dust structure is irregular and non uniform in morphological point of view. The study of Gaussian distribution also indicates high disturbance from background sources.

There is linear relation between the intensity of infrared fluxes in both IRIS and AKARI data with very good correlation coefficient. Furthermore, an inverse relation is observed between dust color temperature and spectral emissivity index in both data. It can be concluded that the high radiation sources within and outside the dust structure are playing major role for the asymmetrical distribution of infrared flux and dust color temperature.

ACKNOWLEDGMENTS

FIGURE 6. Figure shows the Gaussian distribution for intensity of infrared fluxes at 60 μm (a) and 100 μm (b), dust color temperature (c) and dust mass (d) based of IRIS data. In all figure the quantities (flux at 60 μm, 100 μm, dust color temperature, and mass) are taken along X-axis and their PDF are taken along Y-axis.

EDITOR'S NOTE

This manuscript was submitted to the Association of Nepali Physicists in America (ANPA) Conference 2021 for publication in the special issue of Journal of Nepal Physical Society.

REFERENCES

1. M. Matsuura, E. Dwek, M. Meixner, M. Otsuka, B. Babler, M. Barlow, J. Roman-Duval, C. Engelbracht, K. Sandstrom, M. Lakićević, *et al.*, Science **333**, 1258–1261 (2011).
2. H. L. Gomez, O. Krause, M. Barlow, B. Swinyard, P. Owen, C. Clark, M. Matsuura, E. L. Gomez, J. Rho, M.-A. Besel, *et al.*, Astrophys. J. **760**, 96 (2012).
3. C. Gall, J. Hjorth, D. Watson, E. Dwek, J. R. Maund, O. Fox, G. Leloudas, D. Malesani, and A. C. Day-Jones, Nature **511**, 326–329 (2014).
4. M. Paudel, P. Bhandari, and S. Bhattarai, Journal of Nepal Physical Society **7**, 110–118 (2021).
5. A. Gautam and D. Chhatkuli, Journal of Nepal Physical Society **6**, 97–103 (2020).
6. A. Thapa, M. Paudel, and B. Pant, Journal of Nepal Physical Society **5**, 74–84 (2019).
7. A. Jha and B. Aryal, J. Astrophys. Astron. **39**, 1–7 (2018).
8. D. Green, arXiv preprint arXiv:1409.0637 (2014).
9. M.-A. Miville-Deschênes and G. Lagache, Astrophys. J. Supp. Ser. **157**, 302 (2005).
10. H. Murakami, H. Baba, P. Barthel, D. L. Clements, M. Cohen, Y. Doi, K. Enya, E. Figueredo, N. Fujishiro, H. Fujiwara, *et al.*, Publ. Astron. Soc. Japan **59**, S369–S376 (2007).
11. F. Bonnarel, P. Fernique, O. Bienaymé, D. Egret, F. Genova, M. Louys, F. Ochsenbein, M. Wenger, and J. G. Bartlett, Astron. Astrophys. Supp. Ser. **143**, 33–40 (2000).
12. D. O. Wood, P. C. Myers, and D. A. Daugherty, Astrophys. J. Supp. Ser. **95**, 457–501 (1994).
13. S. L. Schnee, N. A. Ridge, A. A. Goodman, and J. G. Li, Astrophys. J. **634**, 442 (2005).
14. R. Assendorp and P. Wesselius, Astron. Astrophy. Supp. Ser. **100**, 473–488 (1993).
15. K. Young, T. Phillips, and G. Knapp, Astrophys. J. **409**, 725–738 (1993).
16. R. H. Hildebrand, Quar. J. R. Astron. Soc. **24**, 267 (1983).
17. T. Henning and H. Mutschke, Astron. Astrophys. **327**, 743–754 (1997).
18. X. Dupac, J.-P. Bernard, N. Boudet, M. Giard, J.-M. Lamarre, C. Mény, F. Pajot, I. Ristorcelli, G. Serra, B. Stepnik, *et al.*, Astron. Astrophys. **404**, L11–L15 (2003).
19. E. Holmberg, Medd. Lund Astron. Obs. Ser. II **117**, 3–82 (1946).
20. M. P. Haynes and R. Giovanelli, Astron. J. **89**, 758–800 (1984).